

BigEarthNet Dataset with A New Class-Nomenclature for Remote Sensing Image Understanding

Gencer Sumbul, *Student Member, IEEE*, Jian Kang, *Member, IEEE*, Tristan Kreuziger, *Student Member, IEEE*, Filipe Marcelino, Hugo Costa, Pedro Benevides, Mario Caetano, Begüm Demir, *Senior Member, IEEE*

Abstract—This paper presents BigEarthNet that is a large-scale Sentinel-2 multispectral image dataset with a new class nomenclature to advance deep learning (DL) studies in remote sensing (RS). BigEarthNet is made up of 590,326 image patches annotated with multi-labels provided by the CORINE Land Cover (CLC) map of 2018 based on its most thematic detailed Level-3 class nomenclature. Initial research demonstrates that some CLC classes are challenging to be accurately described by considering only Sentinel-2 images. To increase the effectiveness of BigEarthNet, in this paper we introduce an alternative class-nomenclature to allow DL models for better learning and describing the complex spatial and spectral information content of the Sentinel-2 images. This is achieved by interpreting and arranging the CLC Level-3 nomenclature based on the properties of Sentinel-2 images in a new nomenclature of 19 classes. Then, the new class-nomenclature of BigEarthNet is used within state-of-the-art DL models in the context of multi-label classification. Results show that the models trained from scratch on BigEarthNet outperform those pre-trained on ImageNet, especially in relation to some complex classes including agriculture, other vegetated and natural environments. All DL models are made publicly available at <http://bigearth.net/#downloads>, offering an important resource to guide future progress on RS image analysis.

Index Terms—Sentinel-2 multispectral images, Land cover land use, Multi-label image classification, Deep neural network, Remote sensing



1 INTRODUCTION

IN recent years, research and applications in the field of deep learning (DL) have made huge leaps and achieved very high performance on a wide variety of tasks, such as image classification, object detection, and natural speech recognition. These advances have attracted the attention of research into modelling the high-level semantic content of remote sensing (RS) images. The rise of DL in different research fields has been made possible due to the availability of large data archives and growing computational power. As an example, the advances in satellite technologies have increased the availability of images regularly acquired by satellite-borne sensors, while the new policies related to free availability of data (e.g., ESA Sentinel missions) support researchers to have access to massive datasets in RS. This creates the potential of DL studies for monitoring the Earth surface, e.g., for climate change analysis, urban area studies, risk and damage assessment, crop monitoring [1], [2].

However, most of the DL models require a huge amount of annotated RS images during training to adjust all parameters and reach high performance. The availability and quality of such data determine the feasibility of many DL

models. The process of collecting, preparing, and annotating RS images at large-scale to create sufficiently large high-quality dataset to drive DL studies is time consuming, complex, and costly in operational scenarios. Therefore, most researchers rely on existing datasets to employ and develop DL methods. However, to the best of our knowledge, there are only few publicly available benchmark datasets in RS. For an overview, the reader is referred to Table 1. Most of the existing datasets feature a relatively small volume of images, which is a limitation for DL based studies due to the above-mentioned reasons. To overcome this problem, a common approach is to exploit DL models with proven architectures (such as ResNet [5] or VGG [6]), which are pre-trained on publicly available general purpose computer vision (CV) datasets (e.g., CIFAR [7] and ImageNet [3]). The existing model is then fine-tuned on a small set of annotated RS images to calibrate the final layers. This saves researchers and developers valuable time by not training models from scratch and even enables more general models. By now, there are several versions of such models that have been pre-trained on large-scale CV datasets used for common DL tasks. However, we argue that this is not a viable approach in RS, because of the differences in image characteristics in CV and RS. As an example, Sentinel-2 multispectral images have 13 spectral bands associated to varying and lower spatial resolutions with respect to CV images (see Fig. 1 for an example of ImageNet and Sentinel-2 images). Additionally, the semantic content present in CV and RS images is also significantly different, and thus their class labels differ from each other. In addition, RS benchmark datasets mostly

- Gencer Sumbul, Jian Kang, Tristan Kreuziger and Begüm Demir are with Technische Universität Berlin, Berlin, Germany.
- Filipe Marcelino, Hugo Costa, Pedro Benevides and Mario Caetano are with Direo-Geral do Territrio, Lisbon, Portugal. Hugo Costa and Mario Caetano are also with NOVA Information Management School (NOVA IMS), Universidade Nova Lisboa, Campus de Campolide, 1070-312 Lisbon, Portugal.

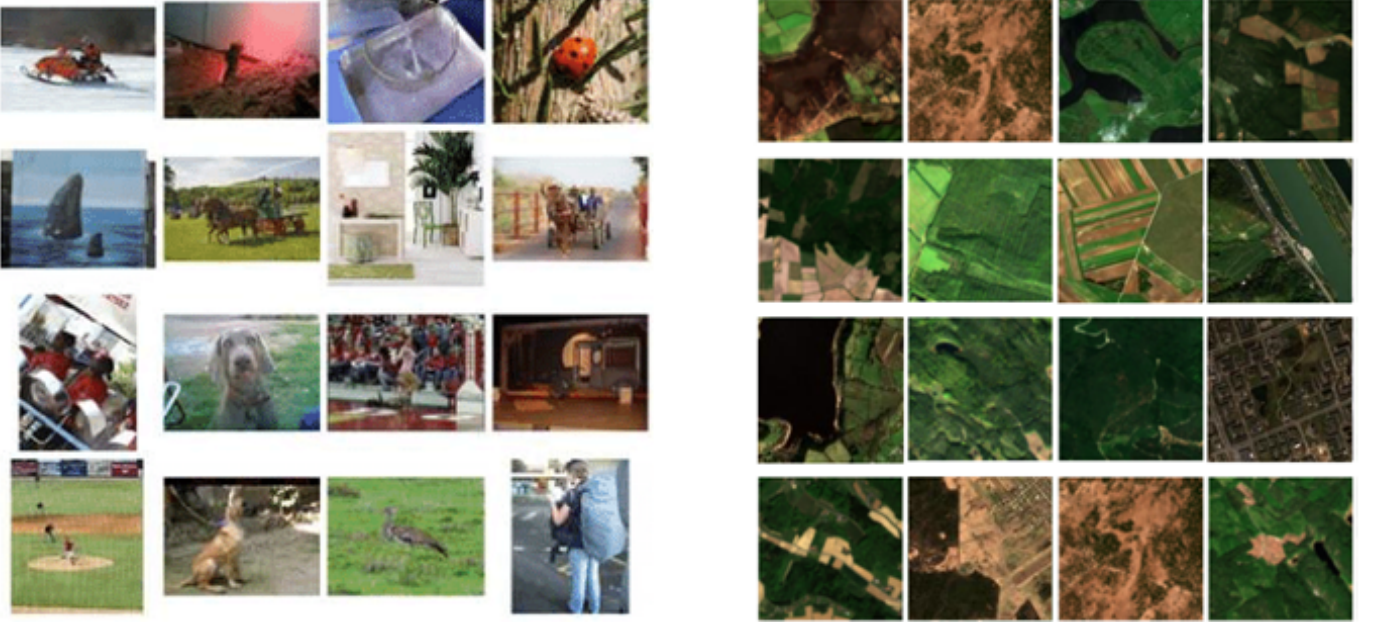


Fig. 1. An example of images from ImageNet [3] (left) and BigEarthNet [4] (right) to show their semantic differences.

contain single-label image annotations, i.e., each image is annotated by a single high level land-use category label that is associated to the most significant content of the considered image. However, RS images usually contain areas with a high variety of semantically complex content that must be reflected by more than one class annotation through low-level class labels (i.e., multi-labels). Thus, a benchmark dataset consisting of images annotated with multi-labels is required. The dataset presented in [8] contains aerial images with multi-labels, however the number of images in this dataset is very small and thus not fully suitable for DL based research.

This lack of large-scale publicly available benchmark datasets of RS images with multi-labels prevents the wide spread adoption of DL models in RS applications, even though raw data and potential applications do exist. To address this issue, we have recently introduced BigEarthNet [4] as a large-scale benchmark dataset for RS image understanding¹. BigEarthNet contains 590,326 image patches, each of which is annotated with multi-labels provided by the CORINE Land Cover (CLC) map of 2018 (CLC 2018) [20]. The CLC nomenclature includes land cover and land use classes grouped in a three-level hierarchy, and BigEarthNet image patches considers the most thematic detailed Level-3 class nomenclature. However, there are some CLC classes that are difficult to identify by only exploiting (single-date) Sentinel-2 images, because: i) land use concepts associated to some classes (e.g., *Dump sites*, *Sport and leisure facilities*) may not be visible from space or fully recognizable with the spatial resolution of Sentinel-2 images, and ii) RS time series, which BigEarthNet does not include, may be required to describe and discriminate some classes (e.g., *Non-irrigated arable land*, *Permanently irrigated land*). To address this problem, in this paper, we propose an

alternative nomenclature for image patches in BigEarthNet as an evolution of the original CLC labels that better express what can be described from (single-date) Sentinel-2 images. In addition, we provide the range of experiments with several well-known state-of-the-art architectures to show the potential of BigEarthNet for scene classification problems. Moreover, we compare the performance of models that have been pre-trained on ImageNet with those that have exclusively been trained on BigEarthNet. A significant contribution of this work is the provisioning of pre-trained models for all discussed architectures, which are publicly available.

The remaining part of this paper is organized as follows. Section 2 introduces the BigEarthNet dataset and its new class nomenclature. Section 3 presents the general problem of multi-label classification and the considered state-of-the-art DL models. Section 4 describes the experimental setup for the evaluation of the given models, while Section 5 illustrates the experimental results. Finally, Section 6 draws the conclusion of this work.

2 BIGEARTHNET AND ITS NEW CLASS-NOMENCLATURE

In this section, we initially describe the BigEarthNet dataset and then introduce the proposed alternative class-nomenclature for images in BigEarthNet.

2.1 BigEarthNet Dataset

BigEarthNet [4] was constructed by 125 Sentinel-2 tiles including images acquired between June 2017 and May 2018 and associated to less than 1% of cloud cover. In detail, Sentinel-2 data are distributed in a tile-based system that segments the globe in 110×110 km related to the UTM coordinate system. The 125 tiles considered in BigEarthNet are scattered over 10 different European countries (Austria,

1. BigEarthNet is available at <http://bigearth.net/>.

TABLE 1
A List of Existing RS Datasets

Dataset Name	Image Type	Annotation Type	Number of Images	Year of Publication
UC Merced [9]	Aerial RGB	Single Label	2,100	2010
UC Merced [8]	Aerial RGB	Multi Label	2,100	2018
WHU-RS19 [10]	Aerial RGB	Single Label	1,005	2013
RSSCN7 [11]	Aerial RGB	Single Label	2,800	2015
SIRI-WHU [12]	Aerial RGB	Single Label	2,400	2016
RSC11 [13]	Aerial RGB	Single Label	1,232	2016
AID [14]	Aerial RGB	Single Label	10,000	2017
NWPU-RESISC45 [15]	Aerial RGB	Single Label	31,500	2017
RSI-CB [16]	Aerial RGB	Single Label	36,707	2017
PatternNet [17]	Aerial RGB	Single Label	30,400	2018
EuroSat [18]	Satellite Multispectral	Single Label	27,000	2019
DFC15 [19]	Aerial RGB	Multi Label	3,342	2019

Belgium, Finland, Ireland, Kosovo, Lithuania, Luxembourg, Portugal, Serbia, Switzerland). All tiles were atmospherically corrected by employing Sentinel-2's Level 2A product generation and formatting tool (sen2cor) provided by ESA. The 10th band of Sentinel-2 has been excluded as it does not contain information on the Earth's surface. Then the tiles were divided into 590,326 non-overlapping image patches, which are denoted as images from now on. Each image is a section of: 1) 120×120 pixels for 10m bands; 2) 60×60 pixels for 20m bands; and 3) 20×20 pixels for 60m bands. One important goal during the tile selection process was to represent all chosen geographic location with images collected in different seasons. Due to the restrictions of finding tiles with a low cloud cover percentage in the relatively narrow time period this has not been possible at each considered location. Accordingly, the following respective numbers of images for autumn, winter, spring, and summer have been selected: 143557, 72877, 175937 and 126913. For Sentinel-2 tiles, the cloud cover percentage is generally higher in winter compared to other seasons. Thus, the number of images in the winter season is the lowest compared to the other seasons. For the quality check of images, visual inspection has also been employed, which led to the identification of 70,987 images that are fully covered by seasonal snow, cloud, and cloud shadow². An example for those cases is shown in Fig. 2. It is recommended that these images are not included into training and test sets for machine learning or DL algorithms particularly when scene classification and content-based image retrieval applications are considered.

2.2 Proposed Class-Nomenclature for BigEarthNet

Each image in BigEarthNet is associated with one or more class labels (i.e. multi-labels) extracted from the CORINE land cover map of 2018. CORINE land cover (CLC) is a pioneer adventure initiated in the 80s of the last century to produce harmonised land cover land use (LCLU) maps for the member states of the European Union [21]. Nowadays,

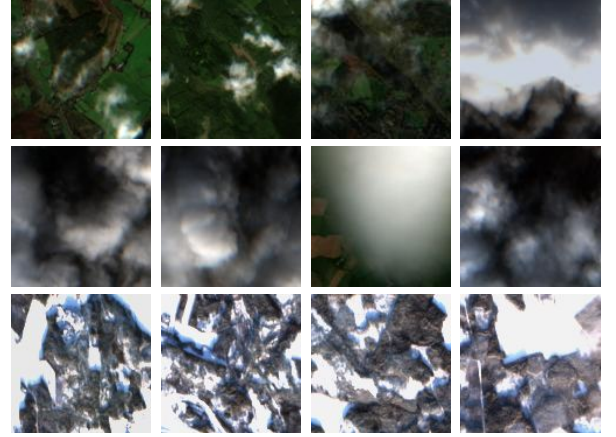


Fig. 2. An example of the BigEarthNet images that are fully covered by seasonal snow, cloud and cloud shadow.

CLC covers 39 countries from Europe and was produced for five reference years, 1990, 2000, 2006, 2012 and 2018. The latter was produced with data of 2017-2018, which matches the time frame of the images included in BigEarthNet.

Motivations for embracing a large-scale mapping endeavour aimed at meeting the demand for spatially explicit and harmonized information on land for a variety of purposes, such as environmental management and decision making [21]. The crude state-of-the-art of the 1980s technology and the large spectrum of potential uses of the maps led to the definition of a coarse spatial resolution and a nomenclature with some broad class definitions mixing land cover and land use concepts. These definitions are implemented for map production by visual interpretation of RS images and auxiliary data in most countries. The same technical specifications were preserved in map updating for historical consistency. Thus the five maps have a minimum mapping unit of 25 ha and a minimum mapping width of 100 m, and provide information on land according to a hierarchical nomenclature of 44 classes at the most detailed level (Level-3). The images in BigEarthNet are representative of 43 CLC

2. The lists of images fully covered by seasonal snow, cloud and cloud shadow are available at <http://bigearth.net/#downloads>.

TABLE 2
Number of Images in BigEarthNet Associated with Each Class for the Proposed Class-nomenclature After Eliminating Images that are Fully Covered by Seasonal Snow, Cloud and Cloud Shadow

Proposed Class-Nomenclature	# of Images
Urban fabric	74,891
Industrial or commercial units	11,865
Arable land	194,148
Pastures	98,997
Permanent crops	29,350
Complex cultivation patterns	104,203
Land principally occupied by agriculture, with significant areas of natural vegetation	130,637
Agro-forestry areas	30,649
Broad-leaved forest	141,300
Coniferous forest	164,775
Mixed forest	176,567
Moors, heathland and sclerophyllous vegetation	16,267
Transitional woodland-shrub	148,950
Beaches, dunes, sands	1,536
Natural grassland and sparsely vegetated areas	12,022
Inland wetlands	22,100
Coastal wetlands	1,566
Inland waters	67,277
Marine waters	74,877

classes.

LCLU classes are possible to map based on human interpretation of imagery and auxiliary data together, but more challenging if only RS images are used. Modifications of the CLC nomenclature are desirable when analysis of observations from space without the help of additional information is of interest. RS systems observe the land cover directly and land use may be inferred from land cover patterns only to a certain extent. This has motivated previous work to adopt modified versions of the CLC nomenclature that better fit the purpose of the application at hand. In [22] CLC is used as a basis to collect training data for supervised image classification, but complex classes such as *Discontinuous urban fabric* were removed. Within a similar supervised image classification framework, in [23] CLC is also used for collecting training data, but complex classes and other classes such as *Sport and leisure facilities* that depend mainly on land use were removed. A deep revision of the CLC program is actually under consideration following the concept of the EIONET Action Group on Land monitoring in Europe (EAGLE) [24].

In this paper, we aim to modify the multi-labels extracted from the CLC 2018 to fit the purpose of training DL models with the Sentinel-2 images archived in BigEarthNet. To this end, the CLC Level-3 nomenclature is interpreted and arranged in a new nomenclature of 19 classes (see Table 2). Ten classes of the original CLC nomenclature are maintained in the new nomenclature, 22 classes are grouped into 9 new classes, and 11 classes are removed. The classes maintained are thematically homogeneous and largely related to land cover, such as *Broad-leaved forest* and *Beaches, dunes, sands*. Furthermore, complex classifications that are often removed when undertaking image classification are maintained, such as



Fig. 3. An example of the BigEarthNet images with their updated multi-labels.

Complex cultivation patterns [23] and *Land principally occupied by agriculture, with significant areas of natural vegetation* [22]. The goal is to investigate the ability of DL models to learn from spatial patterns that express semantic classes. Classes are grouped when sharing similar land cover and spectral patterns. For example, *Moors and heathland* and *Sclerophyllous vegetation* are grouped in a single class, and a new class, *Arable land*, groups similar crops that require dense time series for their discrimination (e.g. irrigated and non-irrigated crops). Grouping classes also increases the number of images available for training as some of the grouped classes are relatively rare, such as *Salines*, which was grouped together with *Salt marshes* in the new class *Coastal wetlands*. Classes that strongly depend on land use or need additional

data for their discrimination are removed. For example, class *Airports* essentially relates to land use, and *Intertidal flats* appear in RS images either with or without water depending on the image acquisition time and hence require appropriate data for its classification. The removed classes tend to be rare and cover a very small proportion of the area of the countries represented in BigEarthNet (<1%). The considered class labels of the new nomenclature and their respective numbers of associated images can be found in Table I. The number of labels associated with each image varies between 1 and 12, while 96.80% of images are not associated with more than 5 labels. Only 23 images are annotated with more than 9 labels. Fig. 3 shows an example of the BigEarthNet images and their new multi-labels.

3 STATE-OF-THE-ART MODELS FOR MULTI-LABEL CLASSIFICATION

Let $\mathcal{X} = \{\mathbf{x}_1, \dots, \mathbf{x}_M\}$ be a dataset consisting of M images, where \mathbf{x}_i is the i -th image in the dataset. Each image in \mathcal{X} is annotated by multi-labels from a label set $\mathcal{L} = \{l_1, \dots, l_S\}$ with $|\mathcal{L}| = S$. Multi-label information of \mathbf{x}_i can be defined by a multi-label vector $\mathbf{y}_i \in \{0, 1\}^S$. If the image is annotated by label l_s , the s -th element of \mathbf{y}_i is set to 1, and 0 otherwise. $\mathcal{Y} = \{\mathbf{y}_1, \dots, \mathbf{y}_M\}$ represents the multi-label set of the dataset. We aim to learn a mapping $F(\mathbf{x}^*; \theta) = g(f(\mathbf{x}^*; \theta))$ based on a multi-label classifier to project a new input image \mathbf{x}^* to multi-labels, where $f(\cdot)$ creates classification scores for each label l_s and $g(\cdot)$ produces \mathbf{y}^* as the predicted multi-label vector, and θ is the set of parameters to be estimated. In this paper, we investigate several state-of-the-art CNN models as multi-label classifiers. Thus, θ becomes the set of parameters of CNNs to be estimated during training. The class probability $P(l_s|\mathbf{x}_i)$ for each class label l_s is determined by applying the *sigmoid* function on the last layer of CNNs with the definition as:

$$P(l_s|\mathbf{x}_i) = \frac{1}{1 + e^{-z_{l_s}}}, \quad (1)$$

where z_{l_s} denotes the class scores. The cross entropy loss is considered to train the CNN models:

$$\sum_{i=1}^M \sum_{s=1}^S [l_s \in \mathbf{y}_i] \log(P(l_s|\mathbf{x}_i)) + (1 - [l_s \in \mathbf{y}_i]) \log(1 - P(l_s|\mathbf{x}_i)), \quad (2)$$

where $[l_s \in \mathbf{y}_i]$ denotes the Iverson bracket, which equals to 1 if $l_s \in \mathbf{y}_i$, and 0 otherwise. The overall loss function (2) can be optimized stochastically based on mini-batches. Mini-batches are defined as subsets of images from the training set to be fed into the CNN models. After an end-to-end training, the set θ of parameters of the CNN models is learned. Then, the CNN models provide the predicted multi-labels \mathbf{y}^* for the new input image \mathbf{x}^* by thresholding the class probabilities [25].

In this section, we investigate several state-of-the-art CNN models, which are: 1) two versions of VGG model [6] that are VGG16 and VGG19; 2) three versions of ResNet model [5] that are ResNet50, ResNet101 and ResNet152; and 3) K-Branch CNN [4] for the classification of BigEarthNet images. In the following, we introduce these models in detail.

3.1 VGG Model

VGG model is a DL model proposed in [6]. It achieved the second place with 92.7% top-5 test accuracy on the ImageNet large-scale Visual Recognition Challenge 2014 (ILSVRC2014) [3]. Its configuration is inspired by AlexNet [26] composed of 5 convolutional layers and 3 fully connected (FC) layers. By increasing the depth of the network (i.e., the number of CNN layers), the VGG model improves the network learning capability with respect to AlexNet. In addition, large filter sizes (e.g., 11×11 and 5×5) in AlexNet are replaced by a small filter size, that is 3×3 . With a certain receptive field, stacking multiple small filters can extract more complex features than the one with a larger filter size at a lower computational cost, since multiple non-linear layers can increase the network depth. In terms of number of CNN layers, there are two versions of VGG model: 1) VGG16 that is composed of 13 convolutional layers and 3 fully connected layers; and 2) VGG19 that is composed of 16 convolutional layers and 3 fully connected layers. The difference between the two versions is that there are three more convolutional layers in the middle part of the network of VGG19 with respect to VGG16. The VGG model has been served as backbone CNN in RS for many tasks, such as poverty mapping [27], building-instance classification [28] and image retrieval [29]. For the multi-label classification with BigEarthNet images, the first layer is adapted to the inputs of multispectral images and the classification layer is changed with respect to the number of classes within the BigEarthNet.

3.2 ResNet Model

The Residual neural network (ResNet) was proposed in [5] to address the *gradient vanish problem* caused by the increasing depth of a CNN. In detail, simply stacking many convolutional layers usually results in very small gradients at the early layers of CNN models during training. The ResNet model exploits identity shortcut connection, which skips one or more layers to learn residual mappings with respect to the inputs, (which is often termed as *skip connection*). Instead of learning an unknown mapping, which directly maps the inputs to the outputs, a residual block is built for learning its residual mapping and it can be much easier learned as the network goes deeper. Therefore, higher accuracy gains can be achieved by a CNN with stacking residual blocks with respect to the previous plain networks. As introduced in [5], there are two types of residual blocks: (1) normal residual block for ResNet18/34; and (2) "bottleneck" residual block for ResNet50/101/152. Two convolutional filters with the size of 3×3 are utilized in the normal residual block, where the number of feature maps is not changed. With practical considerations, Three convolutional filters with the sizes of 1×1 and 3×3 are exploited in the bottleneck residual block. The two 1×1 convolutions are responsible for reducing the feature dimensions, leading to less computational cost and fewer parameters to train with respect to the three 3×3 convolutional layers. In terms of the depth, the versions of ResNet model can be mainly categorized as: 1) ResNet18; 2) ResNet34; 3) ResNet50; 4) ResNet101; and 5) ResNet152, where the number indicates the specific number of layers in the model. The ResNet

model is also one of the most prevalent CNN models for many RS applications, such as semantic segmentation [30], scene classification [2], and object detection [31]. Similar with VGG model, the first and last layer of the ResNet model are modified for classification of BigEarthNet images.

3.3 K-Branch CNN

The K-Branch CNN [32] is proposed to efficiently model the spatial and spectral content of RS images with a branch-wise CNN architecture when the image bands are associated to different spatial resolutions (e.g., Sentinel-2 images). Each branch of the K-Branch CNN is specifically designed for a particular set of image bands with the same spatial resolution. Accordingly, K is the number of resolutions associated with spectral bands of the image. It is worth noting that if all the bands are associated with the same spatial resolution, the K-Branch CNN turns into a single branch CNN (i.e., $K = 1$). Let ρ_i^k be the k^{th} subset of the image bands for corresponding spatial resolution, where $k \in \{1, 2, \dots, K\}$. Each subset ρ_i^k is fed into different branches of the K-Branch CNN. Let ϕ^k be the k^{th} branch, which characterizes the descriptor associated with the k^{th} spatial resolution by employing several convolutional layers and a fully connected layer. Different descriptors for all sets of image bands are first characterized and then stacked together. To efficiently exploit information from different branches, stacked descriptors are fed into a new FC layer to provide the final image descriptor. The classification layer is built upon the final image descriptor. Each branch consists of three convolutional layers with 32, 32 and 64 filters with the size of 2×2 , 3×3 or 5×5 filters. The descriptor associated to each spatial resolution and the final image descriptor are all encoded by 128-dimensional vectors. The last layer is adapted to the number of classes in BigEarthNet.

4 EXPERIMENTAL DESIGN

In the experiments, we excluded the image bands associated to 60m spatial resolution (bands 1 and 9) available in the dataset. This is due to the fact these bands are mainly used for cloud screening, atmospheric correction and cirrus detection in RS applications and do not embody a significant amount of information for the characterization of semantic content of RS images. In the experiments, we compared the VGG model [6] and the ResNet model [5] models at various number of layers (VGG16, VGG19, ResNet50, ResNet101, ResNet152) and the K-Branch CNN model [32]. We selected K as 2 for K-Branch CNN due to the fact that the remaining image bands are associated with two different spatial resolutions. Accordingly, for each image in the dataset, we split the remaining image bands into two subsets associated with 10m and 20m spatial resolutions. The first set of bands with 10m spatial resolution (bands 2, 3, 4, and 8) are fed into the first branch of K-Branch CNN, whereas the second set of bands with 20m spatial resolution (5, 6, 7, 8A, 11 and 12) are fed into the second branch. For the VGG and the ResNet models, we applied cubic interpolation to 20m bands in order to stack all bands into one volume, and thus to feed them into each model at various depths. For all models, we added an FC layer including 19 neurons at the end of

the network as the classification layer. To fairly compare all models, we utilized the Adam approach [33] with the initial learning rate of 10^{-3} to decrease the sigmoid cross entropy loss. Except the learning rate and the optimization approach, we employed the same parameters presented in the [5], [6], [32]. We trained all models for 100 epochs on the training set. It is worth noting that employing special learning rate to each model with appropriate weight decay strategy and utilizing early stopping based on the different metric results on the validation set can further improve the multi-label classification performance of each model. We also compared two different learning strategies: i) learning directly from the BigEarthNet images with ResNet50 and ResNet152; and ii) applying knowledge transfer from ImageNet to the BigEarthNet images by using the pre-trained ResNet50 and ResNet152. Since pre-trained models were trained with RGB channels, we selected only these channels to be used in pre-trained models. Additionally, we also excluded the classification layer from the pre-trained models (which was learnt for ImageNet) and added an FC layer to the end of each model. Then, we applied fine-tuning with 10 epochs only to the classification layer at the end.

To construct train, validation and test sets, images in BigEarthNet can be randomly selected and assigned to the associated sets. However, since images are associated with multi-labels, this approach may not be reliable due to the possibility of not representing in each set all the classes of the whole BigEarthNet. To address this problem, we initially considered four adjacent images acquired within a $2.4\text{km} \times 2.4\text{km}$ area, each of which is associated to an area of $1.2\text{km} \times 1.2\text{km}$. Then, we assigned two of them to the training set, one of them to the validation set and one of them to the testing set. This was applied to all images in the BigEarthNet. Images acquired on the same geographical area at different times (multi-temporal images associated to different seasons) are always included within the same set. By this way, train, validation and test sets do not share the images acquired on the same geographical area. This is very important because we aim that the considered CNN models classify images that are not seen during the training phase. As a result, we finally obtained 269,695 images in the training set, 123,723 images in the validation set and 125,866 in the testing set. It is worth noting that we constructed these sets after eliminating images that are fully covered by seasonal snow, cloud, and cloud shadow. Table 3 shows the number of images of each class associated to training, validation and test sets.

To evaluate the considered models, we employed various classification-based and ranking-based metrics. Classification-based metrics are evaluated based on the list of predicted class labels, while ranking-based metrics also consider the list of probabilities (which is sorted from the highest to the lowest score) for all classes. For the classification metrics, experimental results were given in terms of six metrics: 1) F_1 score; 2) recall (R); 3) precision (P); 4) Jaccard index (J); and 5) Hamming loss (HL). Let tp , fp , fn and tn presents the number of the different prediction conditions true positive, false positive, false negative and true negative, respectively. Accordingly, the recall, the precision and the

TABLE 3
Number of Images of Each Class Associated to Training, Validation and Test Sets

Class	Training	Validation	Test
Urban fabric	38,783	18,180	17,928
Industrial or commercial units	6,182	2,875	2,808
Arable land	100,394	46,604	47,150
Permanent crops	15,862	6,676	6,812
Pastures	50,981	23,846	24,170
Complex cultivation patterns	53,534	25,031	25,638
Land principally occupied by agriculture, with significant areas of natural vegetation	67,260	31,325	32,052
Agro-forestry areas	15,790	7,598	7,261
Broad-leaved forest	73,411	33,759	34,130
Coniferous forest	86,569	38,674	39,532
Mixed forest	91,930	41,996	42,641
Natural grassland and sparsely vegetated areas	6,663	2,560	2,799
Moors, heathland and sclerophyllous vegetation	8,438	3,970	3,859
Transitional woodland-shrub	77,593	35,146	36,211
Beaches, dunes, sands	1,197	118	221
Inland wetlands	11,620	5,131	5,349
Coastal wetlands	1,037	219	310
Inland waters	35,349	15,751	16,177
Marine waters	39,114	17,740	18,023
Total number of images	269,695	123,723	125,866

Jaccard index are defined as follows:

$$R = \frac{tp}{tp + fn}, \quad (3)$$

$$P = \frac{tp}{tp + fp}, \quad (4)$$

$$J = \frac{tp}{tp + fp + fn}. \quad (5)$$

The F_1 score is the harmonic mean of the precision and the recall as follows:

$$F_1 = 2 \times \frac{P \times R}{P + R}. \quad (6)$$

The Hamming loss is the average of Hamming distance calculated among the predicted multi-labels and the ground reference labels. Accordingly, the Hamming loss is defined as follows [34]:

$$HL = \frac{1}{M} \sum_{i=1}^M \frac{1}{S} \sum_{j=1}^S [l_j \in \mathbf{y}_i \oplus l_j \in \mathbf{y}_i^*], \quad (7)$$

where \oplus is the XOR logical operation.

For the ranking-based metrics, experimental results were given in terms of four metrics: 1) Label ranking average precision ($LRAP$); 2) One error (OE); 3) Ranking loss (RL); and 4) Coverage (COV). All these metrics are calculated based on the ranking $rank_{ij}$ of the j^{th} label in the class probabilities list for the i^{th} image \mathbf{x}_i . Accordingly, it is defined as follows:

$$rank_{ij} = |k : P(l_k | \mathbf{x}_i) \geq P(l_j | \mathbf{x}_i)|. \quad (8)$$

The label ranking average precision is evaluated by considering the rate of higher-ranked ground reference labels than each ground reference label. Accordingly, it is defined as follows [35]:

$$LRAP = \frac{1}{M} \sum_{i=1}^M \frac{1}{|\mathbf{y}_i|} \sum_{l_j \in \mathbf{y}_i} \frac{|\{l_k : rank_{ik} \leq rank_{ij}, l_k \in \mathbf{y}_i\}|}{rank_{ij}}. \quad (9)$$

The one error calculates the rate of images, which associated ground reference label does not include the first ranked predicted label. Thus, it is defined as follows [35]:

$$OE = \frac{1}{M} \sum_{i=1}^M [\arg\max_j rank_{ij} \notin \mathbf{y}_i]. \quad (10)$$

The ranking loss calculates the cost of wrongly ordered label pairs (i.e., the probability of a label, which is irrelevant to the image, is higher than a ground reference label). Accordingly, it is defined as follows [36]:

$$RL = \frac{1}{M} \sum_{i=1}^M \frac{1}{|\mathbf{y}_i|(S - |\mathbf{y}_i|)} \sum_{l_j \in \mathbf{y}_i} \sum_{l_k \notin \mathbf{y}_i} rank_{ik} \leq rank_{ij}. \quad (11)$$

The coverage is the average number of labels needed to be associated with the predicted label list such that all ground reference labels will be predicted. Thus, it is calculated as follows [36]:

$$COV = \frac{1}{M} \sum_{i=1}^M \max_{l_j \in \mathbf{y}_i} rank_{ij}. \quad (12)$$

It is worth noting that higher values of the recall, precision, Jaccard index, F_1 score and the label ranking average

TABLE 4
Overall Classification Accuracies Under Different Metrics Obtained by the K-Branch CNN, the VGG16, the VGG19, the ResNet50, the ResNet101 and the ResNet152 on the BigEarthNet Dataset

Metric	K-Branch CNN	VGG16	VGG19	ResNet50	ResNet101	ResNet152
F_1 (%)	72.73	76.01	75.96	77.11	76.49	76.53
R (%)	78.96	75.85	76.71	77.44	77.45	76.24
P (%)	71.61	81.05	79.87	81.39	80.18	81.72
J (%)	62.05	66.12	65.97	67.34	66.66	66.74
HL	0.093	0.077	0.079	0.075	0.077	0.075
$LRAP$ (%)	85.04	87.53	87.42	87.70	87.07	87.73
OE	0.103	0.073	0.071	0.072	0.082	0.072
RL	0.056	0.048	0.048	0.047	0.049	0.046
COV	4.730	4.603	4.606	4.613	4.628	4.552

precision show better performance, whereas smaller values of the Hamming loss, ranking loss, one error and coverage are associated with better performance.

5 EXPERIMENTAL RESULTS

We performed various experiments aiming to analyze: i) the effectiveness of the state-of-the-art CNN models; ii) the class-based performance of these models; and iii) the effectiveness of different learning strategies in the context of multi-label RS image classification.

5.1 Comparison of the Overall Classification Performance of State-of-the-Art CNN Models

In the first set of experiments, we compare the effectiveness of the K-Branch CNN model, VGG model at the depth of 16 and 19 layers (VGG16 and VGG19) and the ResNet model at the depth of 50, 101 and 152 layers (ResNet50, ResNet101, ResNet152) for the multi-label classification of BigEarthNet images. Table 4 shows their overall multi-label classification performance on BigEarthNet under different metrics. By analyzing the table, one can observe that the ResNet model provides the highest scores in most of the metrics. As an example, ResNet152 leads to an increase of about 2% in precision, the ResNet50 achieves a reduction of more than 5% in Hamming loss and ResNet152 provides a reduction of more than 4% in ranking loss compared to VGG19. VGG19 provides the highest score only under the one error with a reduction of less than 2% compared to ResNet50 and ResNet152. This shows that due to the residual connections of the ResNet model and their increased depth in terms of number of layers compared to the VGG model, they achieve better characterization of the semantic content of the BigEarthNet images. In detail, increasing the depth of the VGG model (VGG19) achieves better scores in only recall and one error, and thus provides considerably similar scores in other metrics compared to the shallower version (VGG16). Increasing the depth of the ResNet model from 50 to 101 has similar shortcomings as the VGG model. ResNet101 provides almost the same result with ResNet50 in only recall, whereas ResNet50 achieves a reduction of

more than 4% in ranking loss. However, further increasing the depth of the ResNet model to 152 is capable of increasing the classification performance (while providing better scores under most of the metrics than ResNet50). This shows that only increasing the depth of a CNN model up to some extent is not sufficient to obtain better multi-label classification performance unless the amount of increase allows more accurate characterization of multiple classes present in the image. Moreover, ResNet152 provides better scores compared with the K-Branch CNN. However, the difference is smaller than 4% in recall, Jaccard index, label ranking average precision and F_1 score, whereas the K-Branch CNN model achieves more than 2% recall with significantly reduced number of layers (which is three order of magnitude). This shows that very shallow CNNs can achieve close classification performance to very deep CNNs if the spectral content of RS images is effectively characterized as in K-Branch CNN.

Figure 4 shows an example of BigEarthNet images, their multi-labels and the multi-labels assigned by the K-Branch CNN, VGG16, VGG19, ResNet50, ResNet101 and ResNet152. By analyzing the figure, one can observe that the ResNet model accurately predicts most of the classes with predicting smaller number of wrong classes compared to the K-Branch CNN, VGG16, VGG19. As an example, for the image Fig.4.f, ResNet152 correctly predicts *Urban fabric*, *Industrial or commercial units*, *Transitional woodland-shrub* and *Marine waters* classes. However, the K-Branch CNN and the VGG model are not capable of correctly predicting *Industrial or commercial units* and *Transitional woodland-shrub* classes, respectively. Additionally, for the image Fig.4.c, the ResNet model at all the depths correctly predicts all the classes without predicting any wrong classes in contrast to the K-Branch CNN and the VGG model. In greater details, for the image Fig.4.a, ResNet50 and ResNet101 are capable of accurately characterizing all forest classes present in the image (which are *Agro-forestry areas*, *Broad-leaved forest*, *Mixed forest*) while ResNet152 additionally predict unrelated *Coniferous forest* class. However, other models do not effectively model the different characteristics of all the forest classes, and thus do not accurately predict them. Moreover, K-Branch







	RS Images	Multi-Labels	K-Branch CNN	VGG16	VGG19	ResNet50	ResNet101	ResNet152
a)		urban fabric, arable land, complex cultivation patterns, agro-forestry areas, broad-leaved forest, mixed forest	urban fabric, arable land, complex cultivation patterns, agro-forestry areas, broad-leaved forest, coniferous forest, mixed forest	urban fabric, arable land, agro-forestry areas, broad-leaved forest, coniferous forest	urban fabric, arable land, agro-forestry areas, broad-leaved forest, coniferous forest, mixed forest	urban fabric, arable land, complex cultivation patterns, agro-forestry areas, broad-leaved forest, mixed forest, transitional woodland/shrub	urban fabric, arable land, complex cultivation patterns, mixed forest, transitional woodland/shrub	urban fabric, arable land, complex cultivation patterns, agro-forestry areas, broad-leaved forest, coniferous forest, transitional woodland/shrub
b)		urban fabric, permanent crops, broad-leaved forest, inland waters	industrial or commercial units, mixed forest, inland waters	permanent crops, broad-leaved forest, inland waters	permanent crops, broad-leaved forest, inland waters	urban fabric, permanent crops, broad-leaved forest, inland waters	broad-leaved forest, inland waters	permanent crops, broad-leaved forest, inland waters
c)		arable land, broad-leaved forest, coniferous forest, mixed forest	arable land, agro-forestry areas, broad-leaved forest, natural grassland and sparsely vegetated areas	arable land, broad-leaved forest, coniferous forest, mixed forest	arable land, broad-leaved forest, coniferous forest, mixed forest	arable land, broad-leaved forest, coniferous forest, mixed forest	arable land, broad-leaved forest, coniferous forest, mixed forest	arable land, broad-leaved forest, coniferous forest, mixed forest
d)		urban fabric, arable land, land principally occupied by agriculture, mixed forest, coastal wetlands, marine waters	arable land, complex cultivation patterns, agro-forestry areas, mixed forest, inland wetlands, marine waters	urban fabric, arable land, complex cultivation patterns, mixed forest, inland wetlands, marine waters	urban fabric, arable land, permanent crops, agro-forestry areas, mixed forest, inland wetlands, marine waters	urban fabric, arable land, land principally occupied by agriculture, mixed forest, coastal wetlands, marine waters	urban fabric, arable land, land principally occupied by agriculture, mixed forest, inland wetlands, marine waters	urban fabric, arable land, land principally occupied by agriculture, mixed forest, coastal wetlands, marine waters
e)		arable land, pastures, inland waters	arable land, permanent crops, pastures, inland waters	arable land, natural grassland and sparsely vegetated areas, inland wetlands, inland waters	arable land, natural grassland and sparsely vegetated areas, inland waters	arable land, pastures, inland waters	arable land, pastures, natural grassland and sparsely vegetated areas, inland waters	arable land, pastures, inland waters
f)		urban fabric, industrial or commercial units, transitional woodland-shrub, marine waters	urban fabric, transitional woodland-shrub, marine waters	urban fabric, industrial or commercial units, marine waters	urban fabric, industrial or commercial units, marine waters	urban fabric, industrial or commercial units, marine waters	urban fabric, industrial or commercial units, marine waters	urban fabric, industrial or commercial units, transitional woodland-shrub, marine waters

Fig. 4. An example of the BigEarthNet images with the true multi-labels and the multi-labels assigned by the K-Branch CNN, the VGG16, the VGG19, the ResNet50, the ResNet101 and the ResNet152.

provides *Industrial or commercial units* class as either a wrong prediction or an unrelated prediction as can be seen from the images Fig.4.b and Fig.4.f. These results show that the ResNet model achieves more effective characterization of the semantic content of the BigEarthNet images compared to the K-Branch CNN and the VGG model. However, on a relatively complex scenario like the image Fig.4.d, even the ResNet model is not capable of correctly predicting all classes, which are difficult to simultaneously characterize. As an example, for the *Coastal wetlands* class, ResNet101 wrongly predicts as *Inland wetlands* class. In addition, for the *Land principally occupied by agriculture* class, the VGG16 and the VGG19 wrongly predict as *Complex cultivation patterns* and *Permanent crops* classes, respectively. Moreover, for the image Fig.4.e, although all the models are capable of correctly predicting classes present in the image, they are also predicting unrelated classes (e.g., *Permanent crops*, *Natural grassland and sparsely vegetated areas* and *Inland wetlands*

classes).

5.2 Comparison of the Class-Based Classification Performance With the State-of-the-Art CNN Models

In the second set of experiments, we analyze the class-based classification performance of the K-Branch CNN, VGG16, VGG19, ResNet50, ResNet101 and ResNet152. Table 5 and Table 6 show their classification performance based on each BigEarthNet class under F_1 score and precision, respectively. By analyzing Table 5, one can observe that ResNet50 leads to the best F_1 score on average (which is about 7%, 4%, 2% higher than the K-Branch CNN, VGG19, ResNet101, respectively). In detail, for *Urban fabric*, *Arable land*, *Pastures*, *Broad-leaved forest*, *Coniferous forest*, *Mixed forest* and *Marine waters* classes, the VGG and the ResNet models with varying number of layers achieve similar class-based accuracy with about 2% F_1 score difference between the

TABLE 5
Class-Based Accuracies in F_1 Score (%) Obtained by the K-Branch CNN, the VGG16, the VGG19, the ResNet50, the ResNet101 and the ResNet152 on the BigEarthNet Dataset

Class	K-Branch CNN	VGG16	VGG19	ResNet50	ResNet101	ResNet152
Urban fabric	71.52	74.49	74.45	74.84	74.50	74.32
Industrial or commercial units	38.66	44.41	42.68	48.55	49.11	50.15
Arable land	80.55	82.40	82.04	83.85	82.96	82.92
Permanent crops	47.47	51.53	48.59	51.91	42.35	56.46
Pastures	70.42	70.52	70.46	72.38	71.47	72.35
Complex cultivation patterns	62.68	62.68	61.98	66.03	65.91	64.07
Land principally occupied by agriculture, with significant areas of natural vegetation	59.68	59.61	61.08	60.94	63.41	60.95
Agro-forestry areas	71.30	72.88	72.42	70.49	60.08	74.29
Broad-leaved forest	73.03	73.85	73.14	74.05	73.98	75.36
Coniferous forest	82.73	85.18	84.66	85.41	85.67	85.11
Mixed forest	78.27	78.84	78.77	79.44	80.00	79.64
Natural grassland and sparsely vegetated areas	39.14	40.12	38.58	47.55	49.00	50.92
Moors, heathland and sclerophyllous vegetation	43.79	52.23	54.03	59.41	55.70	46.69
Transitional woodland-shrub	62.46	59.86	60.91	53.47	51.99	60.38
Beaches, dunes, sands	38.71	46.04	42.13	61.46	59.39	58.18
Inland wetlands	48.07	54.65	53.59	60.64	59.10	60.44
Coastal wetlands	19.85	21.15	17.88	47.71	27.26	45.88
Inland waters	74.31	80.39	82.06	83.69	83.40	80.81
Marine waters	88.28	96.55	96.76	97.53	97.77	95.16
<i>Average</i>	60.58	63.55	62.96	67.33	64.90	67.06

highest and lowest scores, whereas K-Branch CNN provides slightly lower scores compared to the other models. However, K-Branch CNN leads to the highest F_1 score for *Transitional woodland-shrub* class with more than 10% higher score compared to ResNet101 and about 9% higher score compared to ResNet50. This shows that effective modeling the *Transitional woodland-shrub* class requires to accurately characterize the spectral content of RS images. Moreover, for *Industrial or commercial units*, *Complex cultivation patterns*, *Natural grassland and sparsely vegetated areas*, *Moors, heathland and sclerophyllous vegetation*, *Beaches, dunes, sands*, *Inland wetlands* and *Coastal wetlands* classes, the ResNet model significantly improves the classification performance compared to the VGG model. In addition, increasing the depth of the ResNet model to 152 further improves the classification performance for comparatively complex classes. As an example, ResNet152 achieves about 8% higher F_1 score for the *Permanent crops* class and more than 12% higher F_1 score for the *Natural grassland and sparsely vegetated areas* class compared to VGG19.

By analyzing Table 6, one can observe that ResNet50 provides the highest score in precision on the average of class based accuracy. As an example, ResNet50 achieves about a 10% higher score in precision compared to VGG19 and more than 10% compared to K-Branch CNN. In contrast to the F_1 score results, the VGG and the K-Branch

CNN models lead to the higher score in precision for the *Industrial or commercial units*, *Arable land*, *Coniferous forest*, *Mixed forest*, *Beaches, dunes, sands*, *Inland waters* and *Marine waters* classes. As an example, VGG16 achieves about 9% higher precision for the *Arable land* class and more than 6% for the *Inland waters* class compared to ResNet101. It is worth noting that F_1 score is the harmonic mean of precision and recall scores. The K-Branch CNN and the VGG models achieve higher scores in precision, whereas providing lower F_1 scores for these classes compared to the ResNet model. This is due to the fact that these models are not capable of providing higher scores in precision together with the recall (which would increase the F_1 score). Thus, these models provide more false negative conditions compared to the false positive conditions. As an example, VGG16 provides more than 3% higher score in precision and more than 5% lower F_1 score compared to the ResNet152 for the *Industrial or commercial units* class.

Irrespective of the differences between the models, complex classes tended to be identified with less accuracy, such as *Industrial and commercial units* and *Permanent crops*. Such classes normally include elements of varying physical properties such as heterogeneous spectral reflectance and atypical spatial distribution, making the detection of consistent patterns useful for classification difficult. Some other cases require dense time series to capture dynamics

TABLE 6
Class-Based Accuracies in Precision (%) Obtained by the K-Branch CNN, the VGG16, the VGG19, the ResNet50, the ResNet101 and the ResNet152 on the BigEarthNet Dataset

Class	K-Branch CNN	VGG16	VGG19	ResNet50	ResNet101	ResNet152
Urban fabric	70.69	76.80	75.90	72.82	78.11	78.80
Industrial or commercial units	47.23	56.25	48.99	53.86	54.70	52.88
Arable land	85.67	86.68	86.54	82.26	77.76	85.37
Permanent crops	43.53	52.49	45.02	76.93	76.73	69.16
Pastures	70.48	75.58	77.38	66.83	68.23	79.56
Complex cultivation patterns	51.14	66.01	64.21	68.23	61.97	70.75
Land principally occupied by agriculture, with significant areas of natural vegetation	56.80	66.36	63.59	64.04	61.45	66.42
Agro-forestry area	61.54	68.16	66.32	82.64	84.11	71.40
Broad-leaved forest	70.45	78.77	75.06	81.03	80.09	73.80
Coniferous forest	80.70	84.64	85.46	83.37	84.48	84.93
Mixed forest	71.03	79.62	77.31	76.90	79.11	78.57
Natural grassland and sparsely vegetated areas	44.25	45.28	48.72	68.53	65.96	56.03
Moors, heathland and sclerophyllous vegetation	52.32	57.67	50.51	68.36	70.11	74.73
Transitional woodland-shrub	50.71	63.65	63.43	70.88	70.81	64.48
Beaches, dunes, sands	93.10	38.82	36.27	66.67	57.38	58.45
Inland wetlands	60	62.88	66.93	73.67	68.70	71.04
Coastal wetlands	39.81	41.51	20.59	82.54	27.76	60.96
Inland waters	72.79	89.09	83.28	84.49	82.75	86.63
Marine waters	98.93	95.99	97.01	96.80	97.21	98.84
<i>Average</i>	64.27	67.70	64.87	74.78	70.92	72.78

for instance caused by tides and frequent land cover change, such as in *Coastal wetlands*. *Agro-forestry areas*, however, presents large scores in F_1 and precision. *Agro-forestry areas* is a class typical of south Europe and mostly present in Portugal among the countries included in BigEarthNet. It corresponds mainly to stands of cork oak and holm oak trees of varying density with annual agriculture or pastures in the understory. The scattered spatial arrangement of the tree-cover provides spatial patterns potentially useful for DL models while more traditional supervised classification methods require dense time series and texture analyses for achieving reasonable results [37], [38]. This shows that state-of-the-art DL models are able to classify complex and difficult classes based on limited time series of spectral data as long as patterns are discernible from RS images.

5.3 Comparison among the Strategies of Transfer Learning from the ImageNet and Learning directly from the BigEarthNet

In the third set of experiments, we compare the effectiveness of learning multi-label classification by only utilizing BigEarthNet images (i.e., training from scratch) with transferring the classification knowledge already learnt on computer vision images (i.e., using the pre-trained model weights learnt on ImageNet) on the class-based classification accuracy. Table 7 shows the class-based F_1 scores

obtained by the pre-trained ResNet50 as well as ResNet50 trained on BigEarthNet. By analyzing the table, one can see that learning from BigEarthNet with ResNet50 achieves more than 17% higher F_1 score on average compared to the transfer learning strategy. As an example, ResNet50 trained from scratch provides more than 6% higher score for the *Industrial or commercial units* class and results almost 12% higher score for the *Complex cultivation patterns* class compared to the pre-trained ResNet50. The main reasons of the success of learning from BigEarthNet with respect to direct application of a transfer learning strategy are threefold. First, utilizing the pre-trained models limits to accurately characterize the spectral content of RS images, since they can only operate on RGB image bands. Second, transferring the knowledge of computer vision classes into the land-cover classes associated to RS images can not be efficiently achieved most of time since complex semantic content of RS images is not present in CV images. Third, pre-trained models are trained for single-label scenario, limiting to effectively characterize the multiple land cover classes present in the RS image. These factors can be identified in comparatively complex land-cover classes. As an example, learning from the BigEarthNet images achieves more than 46% higher F_1 score for the *Moors, heathland and sclerophyllous vegetation* class and more than 68% higher F_1 score for the *Agro-forestry areas* class compared to the transfer learning

TABLE 7
Class-Based Accuracies in F_1 Score (%) Obtained by the Pre-trained ResNet50 and the ResNet50 on the BigEarthNet Dataset

Class	Pre-trained ResNet50	ResNet50
Urban fabric	63.88	74.84
Industrial or commercial units	42.40	48.55
Arable land	80.16	83.85
Permanent crops	24.51	51.91
Pastures	64.50	72.38
Complex cultivation patterns	54.02	66.03
Land principally occupied by agriculture, with significant areas of natural vegetation	51.78	60.94
Agro-forestry areas	2.26	70.49
Broad-leaved forest	56.92	74.05
Coniferous forest	76.54	85.41
Mixed forest	72.07	79.44
Natural grassland and sparsely vegetated areas	27.29	47.55
Moors, heathland and sclerophyllous vegetation	13.23	59.41
Transitional woodland-shrub	42.82	53.47
Beaches, dunes, sands	55.87	61.46
Inland wetlands	35.69	60.64
Coastal wetlands	21.14	47.71
Inland waters	67.20	83.69
Marine waters	94.30	97.53
<i>Average</i>	49.82	67.33

strategy.

Table 8 shows the class-based F_1 scores obtained by the pre-trained ResNet152 as well as the ResNet152 trained on BigEarthNet. By analyzing the table, one can observe that increasing the depth of the pre-trained ResNet model (which achieves higher performance on ImageNet compared to the shallower ResNet architectures) does not improve the class-based classification accuracy on average. Similar to the case with ResNet50, learning from BigEarthNet with ResNet152 significantly increases the classification performance compared to the transfer learning with ResNet152. As an example, training from scratch with ResNet152 achieves about 23% higher F_1 score for the *Permanent crops* class, more than 8% higher score for the *Land principally occupied by agriculture, with significant areas of natural vegetation* class and about 73% higher score for the *Agro-forestry areas* class compared to the pre-trained ResNet152. This shows that using a transfer learning strategy with state-of-the-art models (which are pre-trained on computer vision images) for the multi-label classification of RS images significantly limits the accurate characterization of the semantic content of RS images. This is due to the different characteristics of computer vision images and RS images.

6 CONCLUSION

In this paper, we have presented BigEarthNet, which is a benchmark dataset for RS image understanding with

590,326 Sentinel-2 multispectral image patches annotated with multi-labels from a new class-nomenclature. The aim of the new class-nomenclature is to allow machine learning models for better learning and describing the semantic content of the Sentinel-2 images. To this end, we reorganized CLC class labels to pay more justice to the properties of Sentinel-2 images in BigEarthNet versus the originally provided CLC labels. The new nomenclature includes 19 classes less dependent on land-use concepts that can be better recognized from multi-spectral data. However, some complexity was allowed to remain so to investigate the ability of DL models to learn from spatial patterns that express semantic classes. In this paper, we have also provided a wide variety of results to show the performance of state-of-the-art DL models trained on BigEarthNet in the framework of the multi-label classification of BigEarthNet images. Different architectures, such as the K-Branch CNN model, the VGG model at the depth of 16 and 19 layers (VGG16 and VGG19) and the ResNet model at the depth of 50, 101 and 152 layers (ResNet50, ResNet101, ResNet152), have been chosen to show the viability of the BigEarthNet dataset. One very significant outcome of the experimental results is the success of the models trained from scratch on BigEarthNet when compared to those pre-trained on ImageNet. This is due to the fact that Sentinel-2 images differ significantly in their characteristics (associated to different spatial and spectral resolutions with a much higher number of spectral bands)

TABLE 8
Class-Based Accuracies in F_1 Score (%) Obtained by the Pre-trained ResNet152 and the ResNet152 on the BigEarthNet Dataset

Class	Pre-trained ResNet152	ResNet152
Urban fabric	63.39	74.32
Industrial or commercial units	42.38	50.15
Arable land	80.05	82.92
Permanent crops	23.13	56.46
Pastures	64.88	72.35
Complex cultivation patterns	51.55	64.07
Land principally occupied by agriculture, with significant areas of natural vegetation	51.23	60.95
Agro-forestry areas	1.31	74.29
Broad-leaved forest	56.25	75.36
Coniferous forest	76.23	85.11
Mixed forest	71.26	79.64
Natural grassland and sparsely vegetated areas	32.94	50.92
Moors, heathland and sclerophyllous vegetation	12.93	46.69
Transitional woodland-shrub	40.68	60.38
Beaches, dunes, sands	54.77	58.18
Inland wetlands	36.02	60.44
Coastal wetlands	20.94	45.88
Inland waters	66.26	80.81
Marine waters	94.23	95.16
<i>Average</i>	49.50	67.06

compared to images found in traditional computer vision datasets. This is particularly visible in the presence of some complex classes including agriculture and other vegetated and natural environments.

BigEarthNet makes a significant advancement for the use of DL in RS by overcoming the current limitations of the existing datasets and it opens up promising directions to advance research for the analysis of large-scale RS image datasets. Although in this paper BigEarthNet has been used for multi-label scene classification problems, it is very suitable to be exploited also for information retrieval problems such as: i) large-scale content-based image search and retrieval; and ii) tag based image search and retrieval. As an example, one can research on learning with imbalanced data due to the uneven distribution of land-cover class frequencies. As another example, BigEarthNet is ideal for the transfer learning-based research, since it currently contains only Sentinel-2 images from a selection of European countries. In addition, due to the availability of increased numbers of images regularly acquired by satellite-borne sensors without any image annotations, there is a large potential of exploiting BigEarthNet to assess the unsupervised and semi-supervised learning methods for information discovery from big data archives. BigEarthNet is also suitable for research on integration of RS and volunteered geographic information.

As a future development of this work, we plan to reg-

ularly enrich the BigEarthNet dataset by: i) extending it to whole Europe; ii) including Sentinel-1 Synthetic Aperture Radar patches; iii) including different types of auxiliary data (e.g., Digital Elevation Models); iv) including the class-wise appearance percentages in each image.

ACKNOWLEDGMENT

This work is supported by the European Research Council (ERC) through the ERC-2017-STG BigEarth Project under Grant 759764.

REFERENCES

- [1] M. Ponti, A. A. Chaves, F. R. Jorge, G. B. P. Costa, A. Colturato, and K. R. L. J. C. Branco, "Precision agriculture: Using low-cost systems to acquire low-altitude images," *IEEE Computer Graphics and Applications*, vol. 36, no. 4, pp. 14–20, July 2016.
- [2] G. Cheng, J. Han, and X. Lu, "Remote sensing image scene classification: Benchmark and state of the art," *Proceedings of the IEEE*, vol. 105, no. 10, pp. 1865–1883, 2017.
- [3] O. Russakovsky, J. Deng, H. Su, J. Krause, S. Satheesh, S. Ma, Z. Huang, A. Karpathy, A. Khosla, M. Bernstein, A. C. Berg, and L. Fei-Fei, "ImageNet Large Scale Visual Recognition Challenge," *International Journal of Computer Vision (IJCV)*, vol. 115, no. 3, pp. 211–252, 2015.
- [4] G. Sumbul, M. Charfuelan, B. Demir, and V. Markl, "BigEarthNet: A large-scale benchmark archive for remote sensing image understanding," in *IEEE Intl. Geosci. Remote Sens. Symp.*, 2019.
- [5] K. He, X. Zhang, S. Ren, and J. Sun, "Deep residual learning for image recognition," in *IEEE Conf. Comput. Vis. Pattern Recog.*, 2016, pp. 770–778.

- [6] K. Simonyan and A. Zisserman, "Very deep convolutional networks for large-scale image recognition," *Intl. Conf. Learn. Represent.*, 2015.
- [7] A. Krizhevsky, "Learning multiple layers of features from tiny images," *University of Toronto*, 2009.
- [8] B. Chaudhuri, B. Demir, S. Chaudhuri, and L. Bruzzone, "Multilabel remote sensing image retrieval using a semisupervised graph-theoretic method," *IEEE Trans. Geosci. Remote Sens.*, vol. 56, no. 2, pp. 1144–1158, February 2018.
- [9] Y. Yang and S. Newsam, "Bag-of-visual-words and spatial extensions for land-use classification," in *Intl. Conf. Adv. Geogr. Inf. Syst.*, 2010.
- [10] W. Shao, W. Yang, and G. S. Xia, "Extreme value theory-based calibration for the fusion of multiple features in high-resolution satellite scene classification," *Int. J. Remote Sens.*, vol. 34, no. 23, pp. 8588–8602, 2013.
- [11] Q. Zou, L. Ni, T. Zhang, and Q. Wang, "Deep learning based feature selection for remote sensing scene classification," *IEEE Geosci. Remote Sens. Lett.*, vol. 12, no. 11, pp. 2321–2325, November 2015.
- [12] B. Zhao, Y. Zhong, G. Xia, and L. Zhang, "Dirichlet-derived multiple topic scene classification model for high spatial resolution remote sensing imagery," *IEEE Trans. Geosci. Remote Sens.*, vol. 54, no. 4, pp. 2108–2123, April 2016.
- [13] L. Zhao, P. Tang, and L. Huo, "Feature significance-based multibag-of-visual-words model for remote sensing image scene classification," *Journal of Applied Remote Sensing*, vol. 10, no. 3, pp. 1–21, 2016.
- [14] G.-S. Xia, J. Hu, F. Hu, B. Shi, X. Bai, Y. Zhong, L. Zhang, and X. Lu, "AID: A benchmark data set for performance evaluation of aerial scene classification," *IEEE Trans. Geosci. Remote Sens.*, vol. 55, no. 7, pp. 3965–3981, July 2017.
- [15] G. Cheng, J. Han, and X. Lu, "Remote sensing image scene classification: Benchmark and state of the art," *Proc. IEEE*, vol. 105, no. 10, pp. 1865–1883, October 2017.
- [16] H. Li, C. Tao, Z. Wu, J. Chen, J. Gong, and M. Deng, "RSI-CB: A large scale remote sensing image classification benchmark via crowdsourcing data," *arXiv preprint arXiv:1705.10450*, 2017.
- [17] W. Zhou, S. Newsam, C. Li, and Z. Shao, "Patternnet: A benchmark dataset for performance evaluation of remote sensing image retrieval," *ISPRS J. Photogram. Remote Sens.*, vol. 145, pp. 197–209, 2018.
- [18] P. Helber, B. Bischke, A. Dengel, and D. Borth, "EuroSAT: A novel dataset and deep learning benchmark for land use and land cover classification," *IEEE J. Sel. Top. Appl. Earth Obs. Remote Sens.*, vol. 12, no. 7, pp. 2217–2226, July 2019.
- [19] Y. Hua, L. Mou, and X. X. Zhu, "Recurrently exploring class-wise attention in a hybrid convolutional and bidirectional lstm network for multi-label aerial image classification," *ISPRS J. Photogram. Remote Sens.*, vol. 149, pp. 188–199, 2019.
- [20] J. Feranec, T. Soukup, G. Hazeu, and G. Jaffrain, *European Landscape Dynamics: CORINE Land Cover Data*. Boca Raton, FL, USA: CRC Press, 2016.
- [21] Y. Heymann, C. Steenmans, G. Croisille, and M. Bossard, "Technical guide corine land cover," *Luxembourg (Office for Official Publications of European Communities)*, 2000.
- [22] C. Paris, L. Bruzzone, and D. Fernández-Prieto, "A novel approach to the unsupervised update of land-cover maps by classification of time series of multispectral images," *IEEE Trans. Geosci. Remote Sens.*, vol. 57, no. 7, pp. 4259–4277, July 2019.
- [23] P. Leinenkugel, R. Deck, J. Huth, M. Ottinger, and B. Mack, "The potential of open geodata for automated large-scale land use and land cover classification," *Remote Sens.*, vol. 11, no. 19, p. 2249, 2019.
- [24] S. Arnold, B. Kosztra, G. Banko, G. Smith, G. Hazeu, M. Bock, and N. Valcarcel Sanz, "The eagle concept: a vision of a future european land monitoring framework," in *Proceedings 33th EARSeL Symposium towards Horizon*, vol. 2020. Citeseer, 2013, pp. 551–568.
- [25] R.-E. Fan and C.-J. Lin, "A study on threshold selection for multi-label classification," *Department of Computer Science, National Taiwan University*, pp. 1–23, 2007.
- [26] A. Krizhevsky, I. Sutskever, and G. E. Hinton, "Imagenet classification with deep convolutional neural networks," in *Advances in neural information processing systems*, 2012, pp. 1097–1105.
- [27] M. Xie, N. Jean, M. Burke, D. Lobell, and S. Ermon, "Transfer learning from deep features for remote sensing and poverty mapping," in *Thirtieth AAAI Conference on Artificial Intelligence*, 2016.
- [28] J. Kang, M. Körner, Y. Wang, H. Taubenböck, and X. X. Zhu, "Building instance classification using street view images," *ISPRS J. Photogram. Remote Sens.*, vol. 145, pp. 44–59, 2018.
- [29] W. Zhou, S. Newsam, C. Li, and Z. Shao, "Patternnet: A benchmark dataset for performance evaluation of remote sensing image retrieval," *ISPRS J. Photogram. Remote Sens.*, vol. 145, pp. 197–209, 2018.
- [30] N. Audebert, B. Le Saux, and S. Lefèvre, "Beyond rgb: Very high resolution urban remote sensing with multimodal deep networks," *ISPRS J. Photogram. Remote Sens.*, vol. 140, pp. 20–32, 2018.
- [31] S. M. Azimi, E. Vig, R. Bahmanyar, M. Körner, and P. Reinartz, "Towards multi-class object detection in unconstrained remote sensing imagery," in *Asian Conference on Computer Vision*. Springer, 2018, pp. 150–165.
- [32] G. Sumbul and B. Demir, "A novel multi-attention driven system for multi-label remote sensing image classification," in *IEEE Intl. Geosci. Remote Sens. Symp.*, July 2019, pp. 5726–5729.
- [33] D. P. Kingma and J. Ba, "Adam: A method for stochastic optimization," in *Intl. Conf. Learn. Represent.*, 2014, pp. 1–41.
- [34] G. Tsoumakas and I. Katakis, "Multi-label classification: An overview," *Int J. Data Warehousing and Mining*, vol. 3, no. 3, pp. 1–13, 2007.
- [35] M. Zhang and Z. Zhou, "A review on multi-label learning algorithms," *IEEE Trans. Knowl. Data Eng.*, vol. 26, no. 8, pp. 1819–1837, Aug 2014.
- [36] G. Tsoumakas, I. Katakis, and I. Vlahavas, *Mining Multi-label Data*. Springer, 2010, pp. 667–685.
- [37] V. Rodriguez-Galiano, M. Chica-Olmo, F. Abarca-Hernandez, P. Atkinson, and C. Jeganathan, "Random forest classification of mediterranean land cover using multi-seasonal imagery and multi-seasonal texture," *Remote Sens. Environ.*, vol. 121, pp. 93–107, 2012.
- [38] S. Godinho, N. Guiomar, and A. Gil, "Using a stochastic gradient boosting algorithm to analyse the effectiveness of landsat 8 data for montado land cover mapping: Application in southern Portugal," *Int. J. Appl. Earth Obs. Geoinf.*, vol. 49, pp. 151–162, 2016.